Ultrafast oscillating-magnetic-field generation based on electronic-current dynamics

Xiaofan Zhang,[1] Xiaosong Zhu,[1,*] Dian Wang,[1] Liang Li,[1] Xi Liu,[1] Qing Liao,[2] Pengfei Lan,[1] and Peixiang Lu[1,2,†]
[1]*Wuhan National Laboratory for Optoelectronics, Huazhong University of Science and Technology, Wuhan 430074, China*
[2]*Hubei Key Laboratory of Optical Information and Pattern Recognition, Wuhan Institute of Technology, Wuhan 430205, China*

(Received 1 November 2018; published 14 January 2019)

Electronic-current dynamics play an important role in photoinduced processes and magnetooptics. We theoretically demonstrate ultrafast oscillating-magnetic-field generation based on the electronic dynamics from current carrying states irradiated by a nonhelical, linearly polarized laser field. In this driving field, the electronic currents oscillate periodically, which is attributed to the laser-induced energy shift of orbitals. These electronic currents can induce a strong spatial-localized oscillating magnetic field $\mathbf{B}(\mathbf{r}, t)$ of several tens of Teslas (10^4 G) at the center of targets. The frequency of the induced magnetic field ranges from terahertz to petahertz and can be continuously adjusted by varying the driving laser intensity. The optically induced oscillating magnetic fields we demonstrated will serve as a potential tool for investigations of the ultrafast dynamics in magnetic materials and chiral media.

DOI: 10.1103/PhysRevA.99.013414

I. INTRODUCTION

With the progress of laser technology in the past decades, intense ultrashort light pulses have come of age [1]. The high-intensity, ultrashort optical pulses can be generated by the technology of chirped pulse amplification (CPA) [2] (with this work, Mourou and Strickland were awarded the Nobel Prize in Physics in 2018), which paves the way for the field of ultrafast optical science and opens the door to a radically new approach to exploring and controlling processes of the microcosm [3]. Moreover, a broad range of strong-field phenomenon, such as high harmonic generation (HHG), nonsequential double ionization (NSDI), and photoelectron scattering (PS), can be initiated when the intense ultrafast laser field interacts with matters [4–11].

Recently, based on the HHG, the attosecond laser pulse has been available [12–16], which has drawn considerable attention for its possibility for imaging and detection of the electronic structures and ultrafast dynamics in atoms, molecules, or condensed matter with a combination of Å-scale spatial resolution and attosecond temporal resolution [17–20]. For example, the attosecond pulses have been used to resolve the time when an electron exits a tunneling barrier [21], observe the valence electron motion in real time [22], and control the simple chemical reaction in a molecule [23]. Besides, some works have shown that the attosecond UV pulses can efficiently induce the attosecond-magnetic-field pulse in molecules [24–26]. Such an optically induced ultrafast magnetic field can offer new opportunities in many research areas, including inertial confinement fusion [27], molecular paramagnetic bonding [28], nonequilibrium electronic processes [29], and demagnetization processes [30]. However, many magnetic properties and applications are sensitive to the direction of the magnetic field, such as the spin dynamics of the electron [31], optomagnetic switching for writing magnetic bits [32], and ultrafast precessional magnetization reversal [33]. Consequently, in order to manipulate and detect these ultrafast magnetic processes and features, realizing the ultrafast modulation of the direction of the magnetic field becomes urgent.

In this work, based on the ultrafast electronic dynamics initialized by the interaction of the intense midinfrared femtosecond laser pulse with the current carrying state of atoms, we report on the generation of the ultrafast oscillating magnetic field. When the current carrying state is irradiated by an intense linearly polarized laser field, an spatial-localized oscillating magnetic field with an intensity up to 47 Tesla at the center of the atom can be induced. Moreover, the frequency of the induced magnetic field ranges from terahertz to petahertz and can be modulated by the intensity of the driving field. Because of the ultrahigh oscillation frequency of the induced magnetic field, it will stimulate new potential applications, such as studying the ultrafast magnetic dynamics and revealing an ultrafast and efficient pathway for storing information in magnetic memory devices.

II. THEORETICAL MODEL

In our simulation, we numerically solve the two-dimensional (2D) single-active-electron (SAE) time-dependent Schrödinger equation (TDSE) [34] [atomic units (a.u.) are used throughout this work unless otherwise stated]:

$$i\frac{\partial\psi(\mathbf{r},t)}{\partial t} = [H_0(\mathbf{r}) + \mathbf{r}\cdot\mathbf{E}(t)]\psi(\mathbf{r},t). \quad (1)$$

$H_0(\mathbf{r}) = -\frac{1}{2}\nabla_{\mathbf{r}}^2 + V(\mathbf{r})$ is the field free atomic Hamiltonian and $\nabla_{\mathbf{r}}$ denotes the nabla operating the time-dependent atomic

*zhuxiaosong@hust.edu.cn
†lupeixiang@mail.hust.edu.cn

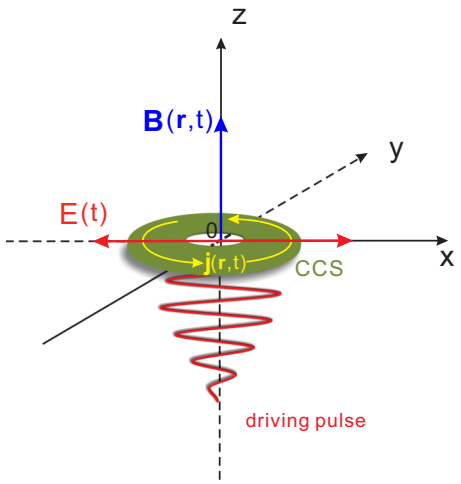

FIG. 1. Illustration of our scheme. We take the initial orbital $2p_+$ as an example and it is indicated by the green annulus. The driving field $\mathbf{E}(t)$ is polarized along x axis, propagating along the z axis. The yellow lines denote the electronic currents $\mathbf{j}(\mathbf{r}, t)$ around the atomic center O in the plane (x, y). The blue line presents the induced magnetic field $\mathbf{B}(\mathbf{r}, t)$ along the z axis and perpendicular to the electronic currents $\mathbf{j}(\mathbf{r}, t)$.

wave packet. $V(\mathbf{r})$ is the atomic Coulomb potential [35]:

$$V(\mathbf{r}) = -\frac{Z(\mathbf{r})}{\sqrt{\mathbf{r}^2 + a}}, \tag{2}$$

where $Z(\mathbf{r}) = 1 + 9\exp(-\mathbf{r}^2)$ is used to account for the screening of the nuclear charge by the inner electrons. A soft parameter $a = 2.88172$ is used to remove the singularity and accurate production of the electronic state potential energies of N_e atom $I_p = 0.793$ for $2p$ orbitals. $\mathbf{r} \equiv (x, y)$ denotes the electron position in the two-dimensional x-y plane. The radiative interaction between the laser field and the electron is described by $\mathbf{r} \cdot \mathbf{E}(t)$ in the length gauge for a linearly polarized laser pulse $\mathbf{E}(t) = E_0 f(t) \cos(\omega t)\mathbf{e}_x$, propagating in the z direction and $\mathbf{e}_x$ is the field polarization direction as shown in Fig. 1 . E_0 and ω are the maximum amplitude and frequency of the pulse. The trapezoidal envelope $f(t)$ is adopted. The current carrying states (CCSs) $2p_\pm$ with magnetic quantum numbers $m = \pm 1$, denoted by $|\varphi_{2p_\pm}\rangle$, are obtained as $|\varphi_{2p_\pm}\rangle = (|\varphi_{2p_x}\rangle \pm i|\varphi_{2p_y}\rangle)/\sqrt{2}$ [35,36], where $|\varphi_{2p_{x,y}}\rangle$ are the two stationary normalized degenerate states obtained by solving TDSE with imaginary time propagation. The CCS can be prepared by a circularly polarized laser pulse propagating along z axis [37]. In the following discussion, we take the CCS $2p_+$ of Ne atom as an example.

The time-dependent electronic current density is defined by the quantum expression in the length gauge [24–26],

$$\mathbf{j}(\mathbf{r}, t) = \frac{i}{2}[\psi(\mathbf{r}, t)\nabla_{\mathbf{r}}\psi^*(\mathbf{r}, t) - \psi^*(\mathbf{r}, t)\nabla_{\mathbf{r}}\psi(\mathbf{r}, t)], \tag{3}$$

where $\psi(\mathbf{r}, t)$ is the exact Born-Oppenheimer (static nuclei) electron wave packet obtained from Eq. (1). Then, the corresponding induced time-dependent magnetic field can be evaluated according to the following classical Jefimenko's equation [38]:

$$\mathbf{B}(\mathbf{r}, t) = \frac{\mu_0}{4\pi}\int\left[\frac{\mathbf{j}(\mathbf{r}', t_r)}{|\mathbf{r} - \mathbf{r}'|^3} + \frac{1}{|\mathbf{r} - \mathbf{r}'|^2 c}\frac{\partial \mathbf{j}(\mathbf{r}', t_r)}{\partial t}\right] \times (\mathbf{r} - \mathbf{r}')d^3\mathbf{r}', \tag{4}$$

where $t_r = t - r/c$ is the retarded time and $\mu_0 = 4\pi \times 10^{-7}$ NA^{-2} (6.692×10^{-4} a.u.). The atomic unit for magnetic field is 1 a.u. $= 2.35 \times 10^5$ T (Tesla). For the induced magnetic field after the laser pulse, Eq. (4) reduces to the classical Biot-Savart law [39] $\mathbf{B}(\mathbf{r}, t) = \frac{\mu_0}{4\pi}\int \frac{\mathbf{j}(\mathbf{r}', t)\times(\mathbf{r}-\mathbf{r}')}{|\mathbf{r}-\mathbf{r}'|^3} d^3\mathbf{r}'$.

III. RESULTS AND DISCUSSIONS

The schematic of our strategy for oscillating-magnetic-field generation is illustrated in Fig. 1. The green annulus on the x-y plane represents the CCS and its angular momentum is along the z axis. When the $2p_+$ state is interacted by the laser field linearly polarized perpendicular to the z direction (as denoted by the red line), the time-dependent wave packet $\psi(\mathbf{r}, t)$ varies periodically between $2p_+$ and $2p_-$ states with opposite angular momentum [40]. The phenomenon of the periodical variation has been interpreted in our previous work Ref. [40]. We have shown that the periodical oscillation of the wave packet is attributed to the different energy shifts of the instantaneous eigenstates, which are parallel and perpendicular to the external field, respectively. Alternatively, this physical process can also be understood by an intuitive interpretation picture, the STIRAP-like process [41]. With the periodical evolution of the time-dependent wave packets, the electronic current oscillates periodically correspondingly, which can induce an oscillating magnetic field.

In Figs. 2(a)–2(f), we display the distributions of the induced electronic current densities $\mathbf{j}(\mathbf{r}, t)$ at different times. The wavelength and intensity of the driving pulse we applied are 1300 nm and 1×10^{14} W/cm^2. The pulse duration is 28 T_0 with a trapezoidal envelope (2 T_0 rising and falling edges and 24 T_0 plateau), in which T_0 is the optical cycle of the driving field. After the pulse, the wave function propagates freely for 2 T_0. The white arrows in Fig. 2 represent the directions of the electronic currents. Here, the counterclockwise direction of electronic current is positive and the clockwise is negative. The direction of the electronic current and the angular momentum of the wave packets satisfy the right-hand rule. From these six distributions, one can clearly see that the directions of the electronic current reverse after t_3. That is, from t_1 to t_3 the direction of the electronic current is positive, while from t_3 to t_6 the direction is negative. It worth nothing that the intensity of the electronic current density $\mathbf{j}(\mathbf{r}, t)$ varies with time. At t_1 and t_4, the intensity is maximum. While, at t_3 and t_6, the intensity is minimum. For better vision of the electronic currents variation, one can examine the dependence of the electronic currents on time by integrating $\mathbf{j}(\mathbf{r}, t)$ over the section from $r = 0$ to $r = \infty$. According to the continuity of the electronic current in quantum mechanics, the probability of the electron being measured through any sections originated from the center point is equal. For convenience, we integrate

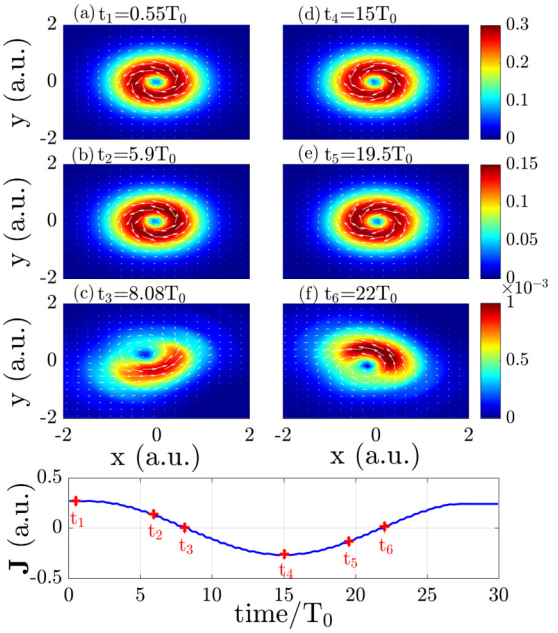

FIG. 2. (a)–(f) The electronic current distributions for different times $t_1 = 0.55T_0$, $t_2 = 5.9T_0$, $t_3 = 8.08T_0$, $t_4 = 15T_0$, $t_5 = 19.5T_0$, and $t_6 = 22T_0$ respectively. The white arrows in (a)–(f) label the directions of the electronic currents. The bottom panel shows the time-dependent electronic currents passing through the section $-\infty - 0$ along y axis. The wavelength and intensity of the driving linear laser field are 1300 nm and 1×10^{14} W/cm^2.

Eq. (3) over the line along the y axis [42,43]

$$\mathbf{J}(t) = \int_{-\infty}^{0} \mathbf{j}(0, y, t) \cdot \mathbf{e}_x dy, \tag{5}$$

where $\mathbf{j}(\mathbf{r}, t) = j_x(\mathbf{r}, t)\mathbf{e}_x + j_y(\mathbf{r}, t)\mathbf{e}_y$ and $\mathbf{e}_{x,y}$ are the unit vector along x and y directions. We present $\mathbf{J}(t)$ in the bottom panel of Fig. 2. The six moments of t_1-t_6 in Figs. 2(a)–2(f) are labeled by the red crosses on the curve. From this figure, one can see that the electronic current oscillates with time resembling a cosine function. The oscillating frequency is about 9 terahertz, which can be adjusted by modulating the intensity of the driving laser field (see the detailed discussion for Fig. 4). According to Eq. (3), the electronic current oscillation is exactly attributed to the wave packet oscillation.

The time-dependent electronic current can be viewed as a time-dependent magnetic dipole, which implies that an internal ultrafast-varying magnetic field can be generated in the atom. In Fig. 3, we display the magnetic field $\mathbf{B}(\mathbf{r}, t)$ induced by the electronic currents $\mathbf{j}(\mathbf{r}, t)$ on the polarization plane (x, y) at different times corresponding to those in Figs. 2(a)–2(f). The blue and red colors, respectively, represent the negative and positive directions of the induced magnetic field along the z direction. From Fig. 3, one can see that the intensity of the magnetic field is maximum at t_1 and t_4, while at t_3 and t_6 the intensity in Figs. 3(c) and 3(f) is minimum, falling down three orders of magnitude compared with that in Figs. 3(a) and 3(d). Moreover, the directions of the induced magnetic field are reversed after t_3, which is attributed to the reversal of the electronic currents after t_3. From t_1 to t_3, the induced magnetic field is toward the negative direction of z axis. While from t_3 to t_6, the direction turns to the positive direction. The intensity variation and the direction reversal of the induced magnetic field are all in accordance with those of the electronic currents in Fig. 2.

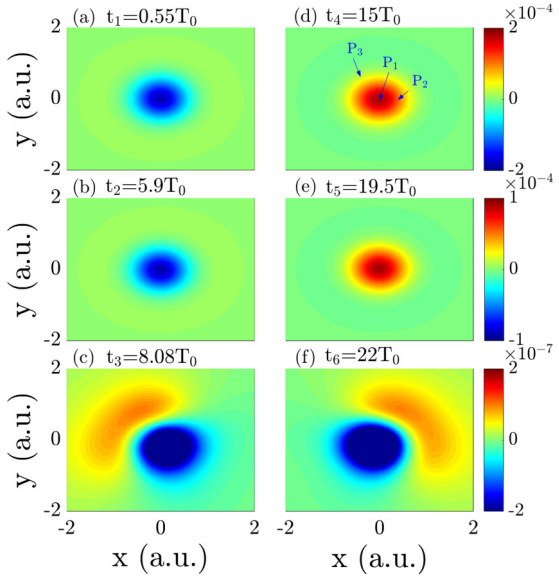

FIG. 3. (a)–(f) The induced magnetic field distribution on the (x, y) plane for different times corresponding to Figs. 2(a)–2(f). The laser parameters are same as those in Fig. 2.

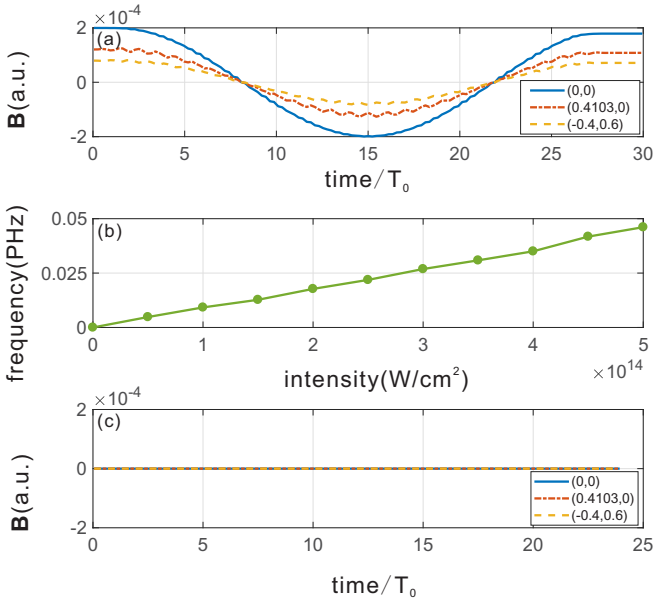

FIG. 4. (a) The induced time-dependent magnetic field of $2p_+$ orbital of Ne atom at three points $P_1(0, 0)$, $P_2(0.4103, 0)$, and $P_3(-0.4, 0.6)$ labeled by the red solid, yellow dash-dot, and blue dashed lines. The laser parameters are the as those in Fig. 2. (b) The oscillation frequencies of the induced magnetic field with different intensities of the driving field and other parameters are the same as those in Fig. 2. (c) The induced time-dependent magnetic field of $1s$ orbital of H atom at the three same points as those in (a). The pulse duration is $24T_0$ and other laser parameters are the same as those in Fig. 2.

For a clearer recognition of the time dependence of the induced magnetic field variation, the intensity of the magnetic field versus time are presented in Fig. 4(a) for three points P_1, P_2, and P_3 labeled by the blue arrows in Fig. 3(d). From Fig. 4(a), one can see that the intensity of the induced magnetic field at the center of the target is maximum and can reach 47 T. With the increase of distance from the central point, the magnetic field intensity decreases. Comparing with the bottom figure in Fig. 2, the induced magnetic field oscillates periodically with the same frequency as that of the electronic currents. As mentioned above, the oscillation of the magnetic field and the electronic current is induced by the periodical evolution of the wave packet, which is essentially attributed to the difference between the energy shifts of the two orbitals parallel and perpendicular to the driving field. The difference of the energy shifts is associated with the oscillation frequency and is dependent on the driving laser intensity. Consequently, one can modulate the oscillation frequency of the magnetic field by continuously adjusting the intensity of the driving laser field. In Fig. 4(b), we present the frequencies of the magnetic field induced by the driving laser field with different intensities. It is shown that the oscillation frequency is almost proportional to the intensity of the driving field. This means that, by adjusting the intensity of the driving field, the frequency can be continuously and linearly modulated from terahertz to subpetahertz. Because the atom we used in our work has a small ionization potential, one cannot excessively increase the intensity of the driving field for a higher oscillation frequency, otherwise the ground state will be depleted due to the high ionization rate. However, one can change the interacted target with larger ionization potential like some cations for a higher oscillation frequency up to petahertz. In addition, we make a comparison between the results from $1s$ and $2p_+$ orbitals and present the magnetic field of the $1s$ orbital of H atom in Fig. 4(c). One can see that the intensity of the induced magnetic field is approximately zero and there is not any oscillation. The comparison indicates that the nonzero angular momentum of the target orbital plays a significant role in generation of the ultrafast oscillating magnetic field.

IV. CONCLUSION

In conclusion, ultrafast oscillating magnetic field generated from the electronic-current dynamics based on the interaction of CCS with intense midinfrared femtosecond laser pulses has been studied by numerically solving TDSE. It has been shown that the frequency of the induced magnetic field can be modulated from terahertz to petahertz by adjusting the intensity of the driving laser field. Our scheme works for CCS in different atoms and molecules. The generation of the ultrafast oscillating magnetic field provides possibility to detect and manipulate the ultrafast magnetic and chiral dynamics, and study electron dynamics in ultrafast magnetooptics. Furthermore, we expect the magnetic source with high oscillation frequency will be applied in other regions, such as the high-speed information processing and storage.

ACKNOWLEDGMENT

This work was supported by National Natural Science Foundation of China (NSFC) under Grants No. 11774109, No. 11574101, No. 11334009, No. 11425414, and No. 11627809.

[1] T. Brabec and F. Krausz, Rev. Mod. Phys. **72**, 545 (2000).
[2] D. Strickland and G. Mourou, Opt. Commun. **56**, 219 (1985).
[3] W. Liu, X. Li, Y. Song, C. Zhang, X. Han, H. Long, B. Wang, K. Wang, and P. Lu, Adv. Funct. Mater. **28**, 1707550 (2018); J. Chen *et al.*, Nano Lett. **18**, 1344 (2018).
[4] J. Vos, L. Cattaneo, S. Patchkovskii, T. Zimmermann, C. Cirelli, M. Lucchini, A. Kheifets, A. S. Landsman, and U. Keller, Science **360**, 1326 (2018).
[5] D. B. Milošević, G. G. Paulus, D. Bauer, and W. Becker, J. Phys. B **39**, R203 (2006).
[6] Y. Mairesse, A. de Bohan, L. J. Frasinski, H. Merdji, L. C. Dinu, P. Monchicourt, P. Breger, M. Kovačev, R. Taïzeb, B. Carré, H. G. Muller, P. Agostini, and P. Salères, Science **302**, 1540 (2003).
[7] B. Wang, L. He, F. Wang, H. Yuan, X. Zhu, P. Lan, and P. Lu, Phys. Rev. A **97**, 013417 (2018).
[8] J. Tan, Y. Zhou, M. He, Y. Chen, Q. Ke, J. Liang, X. Zhu, M. Li, and P. Lu, Phys. Rev. Lett. **121**, 253203 (2018); M. He, Y. Li, Y. Zhou, M. Li, W. Cao, and P. Lu, *ibid.* **120**, 133204 (2018); Y. Zhou, O. I. Tolstikhin, and T. Morishita, *ibid.* **116**, 173001 (2016); J. Tan *et al.*, Opt. Quant. Electron. **50**, 57 (2018).
[9] C. F. M. Faria and X. Liu, J. Mod. Opt. **58**, 1076 (2011).
[10] H. Xie, M. Li, S. Luo, Y. Li, J. Tan, Y. Zhou, W. Cao, and P. Lu, Opt. Lett. **43**, 3220 (2018).
[11] X. Ma, Y. Zhou, N. Li, M. Li, and P. Lu, Opt. Laser Technol. **108**, 235 (2018).
[12] P. M. Paul, E. S. Toma, P. Breger, G. Mullot, F. Augé, Ph. Balcou, H. G. Muller, and P. Agostini, Science **292**, 1689 (2001).
[13] G. Sansone, E. Benedetti, F. Calegari, C. Vozzi, L. Avaldi, R. Flammini, L. Poletto, P. Villoresi, C. Altucci, R. Velotta, S. Stagira, S. De Silvestri, and M. Nisoli, Science **314**, 443 (2006).
[14] L. Li, Z. Wang, F. Li, and H. Long, Opt. Quant. Electron. **49**, 73 (2017).
[15] J. Li, X. Ren, Y. Yin, K. Zhao, A. Chew, Y. Cheng, E. Cunningham, Y. Wang, S. Hu, Y. Wu, M. Chini, and Z. Chang, Nature Commun. **8**, 186 (2017).
[16] T. Gaumnitz, A. Jain, Y. Pertot, M. Huppert, I. Jordan, F. Ardana-Lamas, and H. J. Wörner, Opt. Express **25**, 27506 (2017).
[17] X. Zhu, M. Qin, Y. Li, Q. Zhang, Z. Xu, and P. Lu, Phys. Rev. A **87**, 045402 (2013); X. Zhu, M. Qin, Q. Zhang, Y. Li, Z. Xu, and P. Lu, Opt. Express **21**, 5255 (2013).
[18] H. Yuan *et al.*, Opt. Lett. **43**, 931 (2018); M. Qin and X. Zhu, Opt. Laser Technol. **87**, 79 (2017).
[19] X. Liu, P. Li, X. Zhu, P. Lan, Q. Zhang, and P. Lu, Phys. Rev. A **95**, 033421 (2017).

[20] L. He, P. Lan, A.-T. Le, B. Wang, B. Wang, X. Zhu, P. Lu, and C. D. Lin, Phys. Rev. Lett. **121**, 163201 (2018).
[21] D. Shafir, H. Soifer, B. D. Bruner, M. Dagan, Y. Mairesse, S. Patchkovskii, M. Yu. Ivanov, O. Smirnova, and N. Dudovich, Nature (London) **485**, 343 (2012).
[22] E. Goulielmakis, Z. H. Loh, A. Wirth, R. Santra, N. Rohringer, V. S. Yakovlev, S. Zherebtsov, T. Pfeifer, A. M. Azzeer, M. F. Kling, S. R. Leone, and F. Krausz, Nature (London) **466**, 739 (2010).
[23] P. M. Kraus, B. Mignolet, D. Baykusheva, A. Rupenyan, L. Horný, E. F. Penka, G. Grassi, O. I. Tolstikhin, J. Schneider, F. Jensen, L. B. Madsen, A. D. Bandrauk, F. Remacle, and H. J. Wörner, Science **350**, 790 (2015).
[24] K.-J. Yuan, and A. D. Bandrauk, Phys. Rev. A **92**, 063401 (2015).
[25] K.-J. Yuan, and A. D. Bandrauk, Phys. Rev. A **91**, 042509 (2015).
[26] K.-J. Yuan, J. Guo, and A. D. Bandrauk, Phys. Rev. A **98**, 043410 (2018).
[27] W.-M. Wang, P. Gibbon, Z.-M. Sheng, and Y.-T. Li, Phys. Rev. Lett. **114**, 015001 (2015).
[28] K. K. Lange, E. I. Tellgren, M. R. Hoffmann, and T. Helgaker, Science **337**, 327 (2012).
[29] A. Matos-Abiague and J. Berakdar, Phys. Rev. Lett. **94**, 166801 (2005).
[30] C. La-O-Vorakiat, E. Turgut, C. A. Teale, H. C. Kapteyn, M. M. Murnane, S. Mathias, M. Aeschlimann, C. M. Schneider, J. M. Shaw, H. T. Nembach, and T. J. Silva, Phys. Rev. X **2**, 011005 (2012).
[31] V. M. Edelstein, Phys. Rev. Lett. **80**, 5766 (1998).
[32] C. D. Stanciu, F. Hansteen, A. V. Kimel, A. Kirilyuk, A. Tsukamoto, A. Itoh, and T. Rasing, Phys. Rev. Lett. **99**, 047601 (2007).
[33] F. Hansteen, A. Kimel, A. Kirilyuk, and T. Rasing, Phys. Rev. Lett. **95**, 047402 (2005).
[34] M. D. Feit, J. A. Fleck Jr., and A. Steiger, J. Comput. Phys. **47**, 412 (1982).
[35] I. Barth and M. Lein, J. Phys. B: At. Mol. Opt. Phys. **47**, 204016 (2014).
[36] L. Medisauskas, J. Wragg, H. van der Hart, and M. Y. Ivanov, Phys. Rev. Lett. **115**, 153001 (2015).
[37] S. Eckart, M. Kunitski, M. Richter, A. Hartung, J. Rist, F. Trinter, K. Fehre, N. Schlott, K. Henrichs, L. Ph H. Schmidt, T. Jahnke, M. Schöffler, K. Liu, I. Barth, J. Kaushal, F. Morales, M. Ivanov, O. Smirnova, and R. Dörner, Nature Phys. **14**, 701 (2018).
[38] O. D. Jefimenko, *Electricity and Magnetism: An Introduction to the Theory of Electric and Magnetic Fields*, 2nd ed. (Electret Scientific, Star City, 1989); Am. J. Phys. **58**, 505 (1990).
[39] O. D. Jefimenko, *Electricity and Magnetism: An Introduction to the Theory of Electric and Magnetic Fields* (Electret Scientific, Waynesburg, 1989).
[40] X. Zhang, L. Li, X. Zhu, K. Liu, X. Liu, D. Wang, P. Lan, I. Barth, and P. Lu, Phys. Rev. A **98**, 023418 (2018).
[41] N. V. Vitanov, A. A. Rangelov, B. W. Shore, and K. Bergmann, Rev. Mod. Phys. **89**, 015006 (2017).
[42] H. Mineo, S. H. Lin, and Y. Fujimura, J. Chem. Phys. **138**, 074304 (2013).
[43] H. Mineo and Y. Fujimura, J. Phys. Chem. Lett. **8**, 2019 (2017).